PCCP

PAPER

View Article Online
View Journal | View Issue

Cite this: *Phys. Chem. Chem. Phys.*, 2015, **17**, 10053

Theoretical understanding of two-photon-induced fluorescence of isomorphic nucleoside analogs†

Pralok K. Samanta[a] and Swapan K. Pati*[ab]

Received 9th January 2015,
Accepted 6th March 2015

DOI: 10.1039/c5cp00134j

www.rsc.org/pccp

We use *ab initio* Density Functional Theory (DFT) and Time-dependent DFT (TDDFT) calculations for a detailed understanding of one-photon absorption (1PA) and two-photon absorption (2PA) cross sections of eight different nucleoside analogs. The results are compared and contrasted with the available experimental data. Our calculated results show that the low energy peaks in the absorption spectra mainly arise because of the π–π^* electronic transition of the nucleoside analogs. The emission spectra of the nucleoside analogs are also calculated using TDDFT methods. The calculated absorption and emission spectra in the presence of a solvent follow the same trend as those found experimentally. Our results demonstrate that the nucleoside analogs show significantly different electronic and optical properties, although their bonding aspects towards Watson–Crick base pairing remain the same. We also derive the microscopic details of the origin of nonlinear optical properties of the nucleoside analogs.

1 Introduction

A long chain polymer of amino acids or nucleic acids can be synthesized with artificial residues to introduce new properties to the polymer with the help of a recent advancement in technology.[1,2] This technique helps to replace Watson–Crick base pairing with modified-nucleobase pairing[3–5] or metal-modified base pairing.[6–8] Modified nucleic acid residues possessing fluorescence activity in the UV-visible region improve biological and biomedical applications.[9–12] The natural nucleosides do not show fluorescence in the UV-visible region and hence the modification of nucleosides is important to improve biological and biomedical applications.[13] It is also very important to consider minimal structural and functional perturbations to design a fluorescence active nucleoside analog.[9,14] Therefore, emissive nucleoside analogs that show strong structural resemblance to the natural nucleosides are important.

Molecular two-photon absorption (2PA) has potential applications in spectroscopy, optical data storage,[15] microfabrication,[16] optical power limitation,[17] three-dimensional imaging[18] *etc.* Molecules with efficient 2PA and stimulated emission depletion (STED) are important for enhanced scientific and technological application, such as two-photon-induced fluorescence microscopy (2PFM),[19,20] high-resolution molecular spectroscopy,[21] light amplification of stimulated emission,[22,23] *etc.* Nucleoside analogs with large 2PA cross sections and fluorescence property would have added advantage for biomedical applications. This is because 2PA increased the wavelength of the irradiated light to double in comparison to the 1PA, less (or not) harming the biological cell.

Motivated by the experimental work by Lane *et al.*,[24] here, we explore the photophysical properties of a variety of nucleoside analogs using *ab initio* Density Functional Theoretical (DFT) and Time-dependent DFT (TDDFT) calculations (Fig. 1). These modified nucleosides show fluorescence in the visible region and they also closely resemble the corresponding natural nucleobases with respect to their overall dimensions. These modified nucleosides can form Watson–Crick base pairing with complementary modified or natural nucleosides.[3,4] We calculate 1PA and 2PA properties of these nucleoside analogs. We also calculate their emission spectra and compare with the experimentally reported results. In our study, we provide a microscopic origin of the low-energy 1PA and 2PA peaks and emission peaks that are observed experimentally.

2 Computational details

The geometry of modified nucleosides are optimized using DFT, and their optical spectra are calculated using Time-dependent DFT (TDDFT) methods as implemented in the Gaussian 09 program package.[25] All the calculations are done using B3LYP (Becke, three-parameter, Lee–Yang–Parr)[26–28] hybrid exchange and correlation energy functional, with the 6-31++G(d,p) basis set for all atoms. The DFT and TDDFT calculations are performed both in the gas

[a] *Theoretical Sciences Unit, Jawaharlal Nehru Centre for Advanced Scientific Research, Bangalore 560064, India*
[b] *New Chemistry Unit, Jawaharlal Nehru Centre for Advanced Scientific Research, Bangalore 560064, India. E-mail: pati@jncasr.ac.in; Fax: +91-80-22082767; Tel: +91-80-22082839*

† Electronic supplementary information (ESI) available: Table containing five low energy transition peaks of all the nucleoside analogs in both gas phase and in implicit solvent. See DOI: 10.1039/c5cp00134j

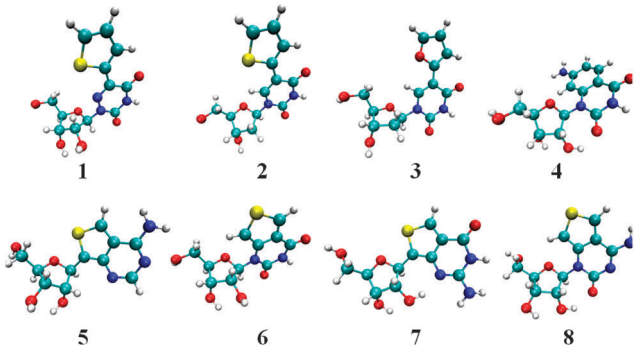

Fig. 1 B3LYP/6-31++G(d,p) level optimized structures of the modified nucleosides and ribonucleosides; **1**: 5-(thiophen-2-yl)-6-aza-uridine, **2**: 5-(thiophen-2yl)-2′-deoxyuridine, **3**: 5-(furan-2-yl)-2′-deoxyuridine, **4**: 7-amino-1-ribosequinozoline-2,4(1*H*,3*H*)-dione. **5**, **6**, **7** and **8** are the thieno[3,4-*d*]pyrimidine nucleoside analogues of A, U, G and C RNA nucleoside, respectively. Atom color code: blue (N), cyan (C), white (H), red (O), and yellow (S).

phase and in a water solvent. Solvent phase calculations are done using the Polarized Continuum Model (PCM).[29] After geometry optimization, frequency calculations are done to remove any vibrational unstable mode. The convergence criterion for the self-consistent-field (SCF) was set to 'Tight', and the 'UltraFine' grid is used for numerical integration in DFT, as implemented in Gaussian 09 sets of code.

The transition intensity for 1PA is described by oscillator strength,

$$f_{ij} = \frac{2\omega_{ij}}{3}\sum_{a}|\langle j|\mu_a|i\rangle|^2 \quad (1)$$

where ω_{ij} denotes the energy difference between the states $|j\rangle$ and $|i\rangle$, and μ_a is the a (x, y or z) component of the dipole moment and the summation is performed over the molecular x, y and z axes.

The 2PA cross section (σ_{2P}) which is directly comparable with experimental measurement is defined as[30–33]

$$\sigma_{2P} = \frac{4\pi^2 {a_0}^5 \alpha \omega^2 g(\omega)}{15 c_0 \Gamma_f}\delta_{2P} \quad (2)$$

where a_0, c_0 and α are the Bohr radius, speed of light and fine structure constant, respectively. ω is the frequency of the incident light, $g(\omega)$ denotes the spectral line profile, Γ_f is the lifetime broadening of the final state.[34]

The 2PA probability (δ_{2P}) of molecules excited by a linearly polarized monochromatic beam is calculated as,[35]

$$\delta_{2P} = 6(S_{xx} + S_{yy} + S_{zz})^2 + 8({S_{xy}}^2 + {S_{xy}}^2 + {S_{xy}}^2 - S_{xx}S_{yy} - S_{xx}S_{zz} - S_{yy}S_{zz}) \quad (3)$$

where $S_{\alpha\beta}$ is the 2P matrix element for the 2P resonant absorption of identical energy. S_{ab} can be calculated using sum-over-state (SOS) formulas,

$$S_{ab} = \sum_j \left[\frac{\langle f|\mu_a|j\rangle\langle j|\mu_b|g\rangle}{\omega_j - \omega_f/2 - i\Gamma_f} + \frac{\langle f|\mu_b|j\rangle\langle j|\mu_a|g\rangle}{\omega_j - \omega_f/2 - i\Gamma_f}\right] \quad (4)$$

where $|g\rangle$ and $|f\rangle$ denote the ground state and final state, respectively, $|j\rangle$ are all the states, ω_j is the excited state energy and μ_a is the a (x, y or z) component of the dipole moment. We have used ten low energy states in our calculations.

The 2PA cross sections of all molecules in both gas phase and solvent phase are calculated with the B3LYP functional using the DALTON2013[36] quantum chemistry program. The 6-31++G(d,p) basis set is used for all the atoms. The PCM model is also considered for solvent phase calculation using DALTON2013. Then the emission spectra are calculated using optimized first excited state (S_1) geometry of each nucleoside analogs using the TDDFT method as implemented in Gaussian 09.[25] Excited state optimizations are done in both gas phase and also in the presence of a solvent (using PCM model), separately. For excited state geometry optimization, the B3LYP exchange and correlation energy functional is used with the 6-31++G(d,p) basis set for all atoms.

3 Results and discussion

3.1 1P absorption

Before discussing the 2PA properties, we discuss the 1PA properties obtained from our TDDFT calculation using the Gaussian 09 program package.[25] While the natural nucleosides show 1PA peak below 300 nm, these nucleoside analogs show 1PA peaks above 300 nm.[3] The 1PA peaks are given in Table 1. We observe the lowest energy peaks at 362 nm, 330, 334 nm and 291 nm for **1–4**, respectively, in water. The lowest energy peaks are found at 345 nm, 304 nm, 339 nm and 322 nm for **5–8**, respectively, and which were reported in water medium in earlier calculations.[3,4] Our calculated lowest energy 1PA peaks are in good agreement with the experimentally observed absorption peaks at 332 nm, 314 nm, 316 nm, 316 nm, 341 nm, 304 nm, 321 nm, and 320 nm, for **1–8**, respectively. We observe that the lowest energy excitation ($S_0 \rightarrow S_1$) corresponds to π–π^* (HOMO $\rightarrow$ LUMO, see Fig. 2) transitions for all the complexes. The red-shifted absorption of these nucleoside analogs compared to natural nucleosides is because of the extended chromophoric system. Like the natural nucleoside, the HOMOs and LUMOs are localized on the nucleobase part of the nucleoside analogs.

Table 1 HOMO–LUMO gap (ΔE_{HL}) and lowest excitation energies ($S_0 \rightarrow S_1$) and corresponding oscillator strengths (f) of all the nucleoside analogs, **1–8** in both gas phase and PCM solvent (water)

	Gas (water) phase	Excitation energy and f				
		Calculated				
	ΔE_{HL}	In gas		In water		Expt.[24,37]
Molecules	eV	eV (nm)	f	eV (nm)	f	eV (nm)
1	3.83 (3.72)	3.48 (356)	0.246	3.42 (362)	0.293	3.73 (332)
2	4.05 (4.21)	3.70 (335)	0.284	3.75 (330)	0.299	3.95 (314)
3	4.08 (4.10)	3.75 (331)	0.283	3.71 (334)	0.313	3.92 (316)
4	4.87 (4.67)	4.40 (282)	0.109	4.26 (291)	0.276	3.92 (316)
5	3.99 (4.02)	3.64 (341)	0.160	3.59 (345)	0.200	3.64 (341)
6	4.71 (4.64)	4.17 (297)	0.066	4.07 (304)	0.085	4.08 (304)
7	4.35 (4.17)	3.86 (321)	0.096	3.66 (339)	0.134	3.86 (321)
8	4.17 (4.40)	3.66 (339)	0.075	3.85 (322)	0.103	3.87 (320)

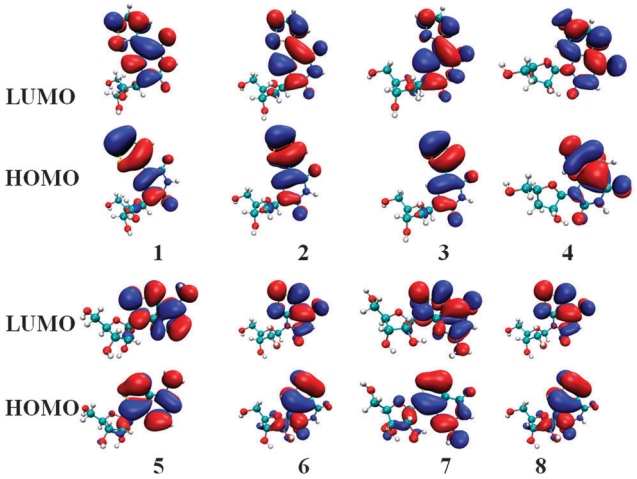

Fig. 2 Calculated highest occupied molecular orbitals (HOMOs) and lowest unoccupied molecular orbitals (LUMOs) of the nucleoside analogs in the gas phase.

3.2 2P absorption

2PA of all the molecules, **1–8**, are also calculated at the B3LYP/6-31++G(d,p) level using DALTON2013 programs.[36] Since the molecules do not have an inversion center, it is expected that 2PA will roughly follow the 1PA spectra (see Fig. 3). We find the same for all the complexes, although the intensity distribution is not the same in 1PA and 2PA (see Table 2). We report five lowest energy excitation ($S_0 \rightarrow S_1$) for both 1PA and 2PA with their transition intensity parameter in Table S1 (see ESI†). $S_0 \rightarrow S_1$ is both 1PA and 2PA active for all the complexes. We find the lowest energy 2PA peaks at 751 nm, 681 nm, 661 nm, 605 nm, 711 nm, 618 nm, 695 nm, and 656 nm, for **1–8**, respectively, in water. Our gas phase calculations give the 1PA peaks for all the molecules (**1–8**) at 356 nm, 335 nm, 331 nm, 282 nm, 341 nm, 297 nm, 321 nm, and 339 nm, respectively and the $S_0 \rightarrow S_1$ 2PA peaks for all the molecules (**1–8**) at 713 nm, 670 nm, 662 nm, 563 nm, 681 nm, 595 nm, 642 nm, and 678 nm, respectively. For both 1PA and 2PA, the transition energies are more or less matching in the solvent phase due to different definition of cavity of solvent molecules in Gaussian 09 and DALTON2013 programs (see Table 2 and Table S1, ESI†). However, the energies are exactly matching in the gas phase for both the programs.[38] Since 2PA increases the wavelength of irradiated light twice (compared to 1PA), it is very much important to excite the molecules using 2P in biological systems. Experimentally, it is reported that the emission spectra of **1–4** and **6** for both 1P and 2P excitation are identical.[24] This means that the emission occurs from the same 2P excited state, which is both 1P and 2P allowed.

3.3 Emission properties

Emission spectra are calculated for all the nucleoside analogs and compared with the experimentally observed emission spectra (see Table 3, Fig. 4). The emission occurs from the first excited state (S_1) and we find the emission peaks at 462 nm, 430, 414 nm, 321 nm for **1–4**, respectively, in water. And the

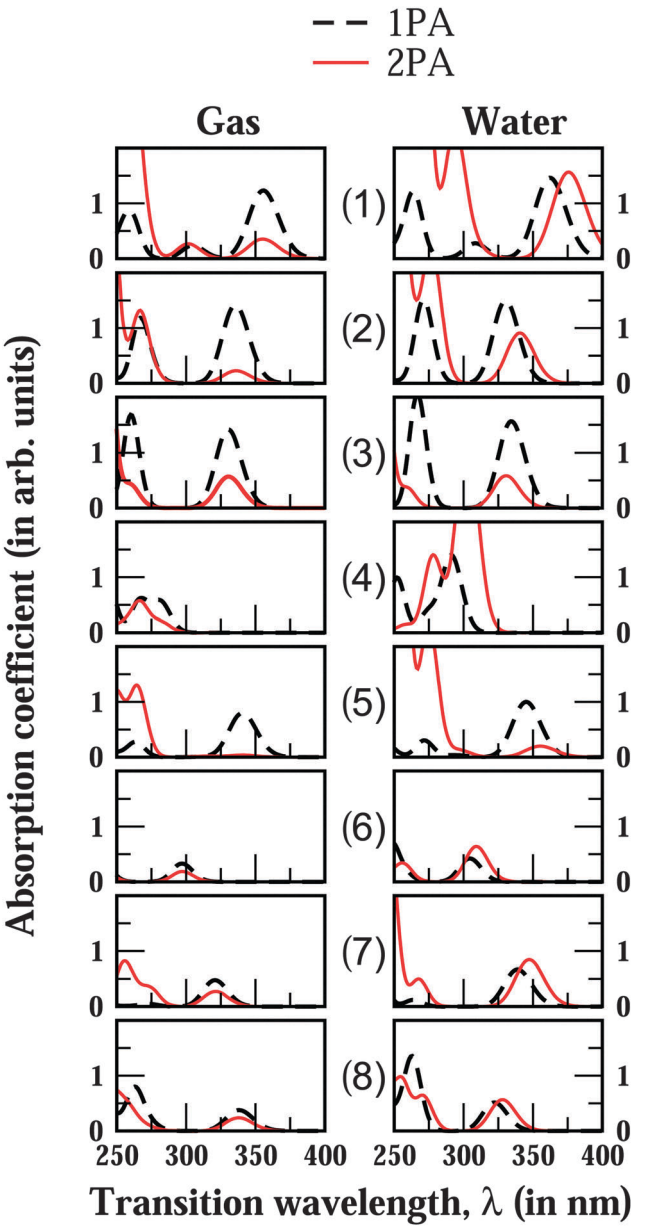

Fig. 3 1PA and 2PA spectra of nucleoside analogs. Half-wavelength is considered for 2PA.

emission peaks are observed at 428 nm, 386 nm, 438 nm, and 443 nm for **5–8**, respectively, and reported earlier in water.[3,4,39] Our calculated emission peaks are in good agreement with the experimentally observed emission peaks at 463 nm, 446 nm, 434 nm, 363 nm, 420 nm, 409 nm, 453 nm, and 429 nm, for **1–8**, respectively, in aqueous solvent.[24,37] These nucleoside analogs show fluorescence in the visible region. On the other hand, natural DNA/RNA nucleosides (A, T, U, G or C) are fluorescence inactive because their excited states decay to the ground state nonradiatively.[40] Our calculated emission peaks in water solvent (using PCM model) are more close to the experimental results compared to the gas phase results. These results also suggest the important roles of solvent in the photophysical properties of these systems.

Table 2 Lowest transition energy peaks ($S_0 \rightarrow S_1$) of the nucleoside analogues, **1–8** in both gas phase and in implicit solvent (water). Oscillator strength (f) for 1PA and σ_{2P} (in GM) for 2PA are also given[a]

	Transition energy							
	Calculated							
	In gas				In water			
	1PA		2PA		1PA		2PA	
Molecules	eV (nm)	f	eV (nm)	σ_{2P}	eV (nm)	f	eV (nm)	σ_{2P}
1	3.48 (356)	0.25	3.49 (713)	7.08	3.42 (362)	0.29	3.30 (751)	31.30
2	3.70 (335)	0.28	3.69 (670)	4.55	3.75 (330)	0.23	3.64 (681)	18.23
3	3.75 (331)	0.28	3.75 (662)	11.36	3.71 (334)	0.31	3.75 (661)	11.70
4	4.40 (282)	0.11	4.40 (563)	3.72	4.26 (291)	0.28	4.10 (605)	72.65
5	3.64 (341)	0.16	4.64 (681)	7.45	3.59 (345)	0.20	3.49 (711)	3.98
6	4.17 (297)	0.07	4.17 (595)	3.74	4.07 (304)	0.08	4.01 (618)	12.82
7	3.86 (321)	0.10	3.86 (642)	5.54	3.66 (339)	0.13	3.57 (714)	16.90
8	3.66 (339)	0.08	3.67 (678)	4.78	3.85 (322)	0.10	3.78 (656)	11.32

[a] For 2PA, the wavelengths are twice the wavelength equivalent to transition energies.

Table 3 Emission peaks ($S_1 \rightarrow S_0$) of all the nucleoside analogs with their corresponding oscillator strength (f) and radiative lifetime (τ)

	Emission energy, f and τ						
	Calculated						
	In gas			In water			Expt.[24,37]
Molecules	eV (nm)	f	τ (ns)	eV (nm)	f	τ (ns)	eV (nm)
1	2.79 (444)	0.151	19.6	2.68 (462)	0.328	9.8	2.68 (463)
2	2.99 (415)	0.221	11.6	2.88 (430)	0.419	6.6	2.78 (446)
3	3.13 (396)	0.224	10.5	2.99 (414)	0.393	6.5	2.86 (434)
4	4.19 (296)	0.132	10.0	3.86 (321)	0.558	2.8	3.42 (363)
5	2.97 (417)	0.132	19.7	2.89 (428)	0.254	10.9	2.95 (420)
6	3.26 (380)	0.049	44.0	3.21 (386)	0.116	19.2	3.03 (409)
7	3.07 (404)	0.079	31.1	2.83 (438)	0.156	18.4	2.74 (453)
8	2.69 (461)	0.053	60.0	2.80 (443)	0.121	24.3	2.89 (429)

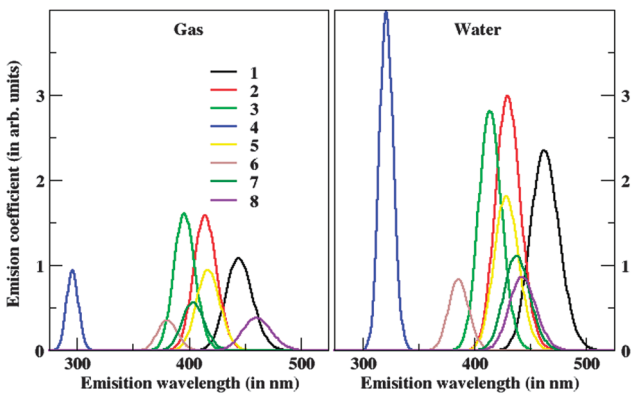

Fig. 4 Calculated emission spectra of the nucleoside analogs in both gas phase and in implicit solvent.

The radiative lifetime (τ) is calculated for spontaneous emission by using the Einstein transition probabilities according to the formula (in a.u.).[41,42]

$$\tau = \frac{c^3}{2(E_{\mathrm{flu}})^2 f} \quad (5)$$

where c, E_{flu} and f are the velocity of light, fluorescence energy and oscillator strength, respectively. The small value of τ indicates the high light-emitting efficiency. This also can be explained in terms of oscillator strength (f). The higher value of τ indicates the electron or energy transfer. The τ-values for all the molecules are shown in Table 3. Our results show that molecule **4** has the lowest τ value among all the molecules and hence has the highest light-emitting efficiency.

4 Conclusions

To summarize, we use DFT and TDDFT calculations with the B3LYP functional and 6-31++G(d,p) basis sets for the detailed understanding of 1PA and 2PA of eight different nucleoside analogs. All the nucleoside analogs are 2PA active and show fluorescence in the visible region. The results are compared against the findings from both gas phase and implicit solvent calculations with the available experimental data. Our calculated results show that the low energy peaks in the absorption spectra mainly arise because of the π–π* (HOMO → LUMO) electronic transition of the nucleoside analogs. The calculated absorption and emission spectra in the presence of solvent are well comparable with the experimental findings. The emission occurs from the same 2P excited state, which is both 1P and 2P allowed. We find that the nucleoside analogs show significantly different electronic and optical properties, although their Watson–Crick

base pairing property remains the same as natural nucleobases (A, U, G and C). Our results give microscopic details of the experimentally observed two-photon stimulated emission of the nucleoside analogs (**1–4**, **6**). Herein, we theoretically predict three nucleoside analogs (**5**, **7** and **8**) having strong two-photon stimulated emission in the visible region. We believe that the nucleoside analogs can be used as sensing probes and have important applications in biological systems as singe-molecule labels.

Acknowledgements

PKS thanks CSIR for Senior Research Fellowship (SRF). SKP acknowledges research support from DST, Government of India and European Union through FP7-Marie Curie Actions: ITN Nano2Fun GA no: 607721.

References

1 R. B. Merrifield, *J. Am. Chem. Soc.*, 1963, **85**, 2149–2154.
2 K. Tanaka and M. Shionoya, *Coord. Chem. Rev.*, 2007, **251**, 2732–2742.
3 P. K. Samanta, A. K. Manna and S. K. Pati, *J. Phys. Chem. B*, 2012, **116**, 7618–7626.
4 P. K. Samanta and S. K. Pati, *New J. Chem.*, 2013, **37**, 3640–3646.
5 A. K. Jissy and A. Datta, *J. Phys. Chem. Lett.*, 2013, **5**, 154–166.
6 G. H. Clever, C. Kaul and T. Carell, *Angew. Chem., Int. Ed.*, 2007, **46**, 6226–6236.
7 P. K. Samanta, A. K. Manna and S. K. Pati, *Chem. – Asian J.*, 2012, **7**, 2718–2728.
8 P. K. Samanta and S. K. Pati, *Chem. – Eur. J.*, 2014, **20**, 1760–1764.
9 R. W. Sinkeldam, N. J. Greco and Y. Tor, *Chem. Rev.*, 2010, **110**, 2579–2619.
10 M. Barbatti, A. J. Aquino, J. J. Szymczak, D. Nachtigallová, P. Hobza and and H. Lischka, *Proc. Natl. Acad. Sci.*, 2010, **107**, 21453–21458.
11 C. T. Middleton, K. de La Harpe, C. Su, Y. K. Law, C. E. Crespo-Hernándezand and B. Kohler, *Annu. Rev. Phys. Chem.*, 2009, **60**, 217–239.
12 Z. Xu, D. R. Spring and J. Yoon, *Chem. – Asian J.*, 2011, **6**, 2114–2122.
13 M. Z. Zgierski, T. Fujiwara, W. G. Kofron and E. C. Lim, *Phys. Chem. Chem. Phys.*, 2007, **9**, 3206–3209.
14 N. J. Greco and Y. Tor, *J. Am. Chem. Soc.*, 2005, **127**, 10784–10785.
15 D. A. Parthenopoulos and P. M. Rentzepis, *Science*, 1989, **245**, 843–845.
16 B. H. Cumpston, S. P. Ananthavel, S. Barlow, D. L. Dyer, J. E. Ehrlich, L. L. Erskine, A. A. Heikal, S. M. Kuebler, I.-Y. S. Lee and D. McCord-Maughon, *et al*, *Nature*, 1999, **398**, 51–54.
17 J. Ehrlich, X. Wu, I. Lee, Z.-Y. Hu, H. Röckel, S. Marder and J. Perry, *Opt. Lett.*, 1997, **22**, 1843–1845.
18 W. Denk, J. H. Strickler and W. W. Webb, *et al*, *Science*, 1990, **248**, 73–76.
19 J. B. Ding, K. T. Takasaki and B. L. Sabatini, *Neuron*, 2009, **63**, 429–437.
20 G. Moneron and S. W. Hell, *Opt. Express*, 2009, **17**, 14567–14573.
21 D. E. Reisner, R. W. Field, J. L. Kinsey and H.-L. Dai, *J. Chem. Phys.*, 1984, **80**, 5968–5978.
22 S. Lattante, G. Barbarella, L. Favaretto, G. Gigli, R. Cingolani and M. Anni, *Appl. Phys. Lett.*, 2006, **89**, 051111.
23 T. Kobayashi, J.-B. Savatier, G. Jordan, W. J. Blau, Y. Suzuki and T. Kaino, *Appl. Phys. Lett.*, 2004, **85**, 185–187.
24 R. S. Lane, R. Jones, R. W. Sinkeldam, Y. Tor and S. W. Magennis, *ChemPhysChem*, 2014, **15**, 867–871.
25 M. J. Frisch, G. W. Trucks, H. B. Schlegel, G. E. Scuseria, M. A. Robb, J. R. Cheeseman, G. Scalmani, V. Barone, B. Mennucci, G. A. Petersson, H. Nakatsuji, M. Caricato, X. Li, H. P. Hratchian, A. F. Izmaylov, J. Bloino, G. Zheng, J. L. Sonnenberg, M. Hada, M. Ehara, K. Toyota, R. Fukuda, J. Hasegawa, M. Ishida, T. Nakajima, Y. Honda, O. Kitao, H. Nakai, T. Vreven, J. A. Montgomery Jr., J. E. Peralta, F. Ogliaro, M. Bearpark, J. J. Heyd, E. Brothers, K. N. Kudin, V. N. Staroverov, R. Kobayashi, J. Normand, K. Raghavachari, A. Rendell, J. C. Burant, S. S. Iyengar, J. Tomasi, M. Cossi, N. Rega, J. M. Millam, M. Klene, J. E. Knox, J. B. Cross, V. Bakken, C. Adamo, J. Jaramillo, R. Gomperts, R. E. Stratmann, O. Yazyev, A. J. Austin, R. Cammi, C. Pomelli, J. W. Ochterski, R. L. Martin, K. Morokuma, V. G. Zakrzewski, G. A. Voth, P. Salvador, J. J. Dannenberg, S. Dapprich, A. D. Daniels, Ö. Farkas, J. B. Foresman, J. V. Ortiz, J. Cioslowski and D. J. Fox, *Gaussian 09 Revision A.01*, GaussianInc, Wallingford CT, 2009.
26 A. D. Becke, *J. Chem. Phys.*, 1993, **98**, 5648–5652.
27 C. Lee, W. Yang and R. G. Parr, *Phys. Rev. [Sect.] B*, 1988, **37**, 785–789.
28 B. Miehlich, A. Savin, H. Stoll and H. Preuss, *Chem. Phys. Lett.*, 1989, **157**, 200–206.
29 G. Scalmani and M. J. Frisch, *J. Chem. Phys.*, 2010, **132**, 114110.
30 C.-K. Wang, P. Macak, Y. Luo and H. gren, *J. Chem. Phys.*, 2001, **114**, 9813–9820.
31 M. Sun, J. Chen and H. Xu, *J. Chem. Phys.*, 2008, **128**, 064106.
32 J.-D. Guo, C.-K. Wang, Y. Luo and H. gren, *Phys. Chem. Chem. Phys.*, 2003, **5**, 3869–3873.
33 F. Todescato, I. Fortunati, S. Carlotto, C. Ferrante, L. Grisanti, C. Sissa, A. Painelli, A. Colombo, C. Dragonetti and D. Roberto, *Phys. Chem. Chem. Phys.*, 2011, **13**, 11099–11109.
34 M. Albota, D. Beljonne, J.-L. Brédas, J. E. Ehrlich, J.-Y. Fu, A. A. Heikal, S. E. Hess, T. Kogej, M. D. Levin and S. R. Marder, *et al.*, *Science*, 1998, **281**, 1653–1656.
35 J. Olsen and P. Jo, *et al*, *J. Chem. Phys.*, 1985, **82**, 3235–3264.
36 K. Aidas, C. Angeli, K. L. Bak, V. Bakken, R. Bast, L. Boman, O. Christiansen, R. Cimiraglia, S. Coriani, P. Dahle, E. K. Dalskov, U. Ekström, T. Enevoldsen, J. J. Eriksen, P. Ettenhuber, B. Fernández, L. Ferrighi, H. Fliegl, L. Frediani, K. Hald, A. Halkier, C. Hättig, H. Heiberg, T. Helgaker, A. C. Hennum, H. Hettema, E. Hjertenæs, S. Høst, I.-M. Høyvik, M. F. Iozzi,

B. Jansík, H. J. A. Jensen, D. Jonsson, P. Jørgensen, J. Kauczor, S. Kirpekar, T. Kjærgaard, W. Klopper, S. Knecht, R. Kobayashi, H. Koch, J. Kongsted, A. Krapp, K. Kristensen, A. Ligabue, O. B. Lutnæs, J. I. Melo, K. V. Mikkelsen, R. H. Myhre, C. Neiss, C. B. Nielsen, P. Norman, J. Olsen, J. M. H. Olsen, A. Osted, M. J. Packer, F. Pawlowski, T. B. Pedersen, P. F. Provasi, S. Reine, Z. Rinkevicius, T. A. Ruden, K. Ruud, V. V. Rybkin, P. Sałek, C. C. M. Samson, A. S. de Merás, T. Saue, S. P. A. Sauer, B. Schimmelpfennig, K. Sneskov, A. H. Steindal, K. O. Sylvester-Hvid, P. R. Taylor, A. M. Teale, E. I. Tellgren, D. P. Tew, A. J. Thorvaldsen, L. Thøgersen, O. Vahtras, M. A. Watson, D. J. D. Wilson, M. Ziolkowski and H. Agren, *Wiley Interdiscip. Rev.: Comput. Mol. Sci.*, 2014, **4**, 269–284.

37 D. Shin, R. W. Sinkeldam and Y. Tor, *J. Am. Chem. Soc.*, 2011, **133**, 14912–14915.

38 Orbitals and transitons energies are exactly matching for same level(B3LYP/6-31++g(d,p)) calculations using either G09 or DALTON-2013 in gasphase. But the energies are more or less matching in solvent phase due todifferent definition of cavity of solvent molecules.

39 M. Gedik and A. Brown, *J. Photochem. Photobiol., A*, 2013, **259**, 25–32.

40 B. Kohler, *J. Phys. Chem. Lett.*, 2010, **1**, 2047–2053.

41 R. C. Hilborn, arXiv preprint physics/0202029, 2002.

42 V. Lukes, A. Aquino and H. Lischka, *J. Phys. Chem. A*, 2005, **109**, 10232–10238.

